Document downloaded from:

http://hdl.handle.net/10251/166366

This paper must be cited as:

Cabrero-Antonino, M.; Albero-Sancho, J.; García-Vallés, C.; Alvaro Rodríguez, MM.; Navalón Oltra, S.; García Gómez, H. (2020). Plasma-Induced Defects Enhance the Visible-Light Photocatalytic Activity of MIL-125(Ti)-NH2 for Overall Water Splitting. Chemistry - A European Journal. 26(67):15682-15689. https://doi.org/10.1002/chem.202003763

The final publication is available at

https://doi.org/10.1002/chem.202003763

Copyright John Wiley & Sons

Additional Information

This is the peer reviewed version of the following article: M. Cabrero-Antonino, J. Albero, C. García-Vallés, M. Álvaro, S. Navalón, H. García, Chem. Eur. J. 2020, 26, 15682, which has been published in final form at https://doi.org/10.1002/chem.202003763. This article may be used for non-commercial purposes in accordance with Wiley Terms and Conditions for Self-Archiving.

Plasma-induced defects enhance the visible-light photocatalytic activity of MIL-125(Ti)-NH_2 for overall water splitting

María Cabrero-Antonino,[a] Josep Albero,[b] Cristina García-Vallés,[a] Mercedes Álvaro,[a] Sergio Navalón,[a],* Hermenegildo García, [b], [c], *

[a] María Cabrero-Antonino, Cristina García-Vallés, Mercedes Álvaro and Sergio Navalón.
Departamento de Química
Universitat Politècnica de València
Camino de Vera s/n, Valencia 46022, Spain
E-mail: sernaol@upvnet.upv.es
[b] Josep Albero and Hermenegildo García.
Instituto Universitario de Tecnología Química
Universitat Politècnica de València
Av. de los Naranjos, Valencia 46022, Spain
[c] Hermenegildo García.
Center of Excellence for Advanced Materials Research
King Abdulaziz University
Jeddah, Saudi Arabia

Supporting information for this article is given via a link at the end of the document.

Abstract: Defect engineering in metal-organic frameworks is commonly performed by using thermal or chemical treatments. Herein, it is reported that oxygen plasma treatment generates structural defects on MIL-125(Ti)-NH_2 leading to an increase of its photocatalytic activity. Characterization data indicates that plasma-treated materials retain most of their initial crystallinity, while exhibiting somewhat lower surface area and pore volume. XPS and FT-IR spectroscopy reveal that oxygen plasma induces MIL-125(Ti)-NH_2 partial terephthalate decarboxylation and an increase of the Ti-OH population. Thermogravimetric analyses confirm the generation of structural defects by oxygen plasma and allowed an estimation of the resulting experimental formula of the treated MIL-125(Ti)-NH_2 solids. SEM analyses show that the oxygen plasma treatment of MIL-125(Ti)-NH_2 gradually decreases its particle size. Importantly, diffuse reflectance UV-Vis spectroscopy and valence band measurements demonstrate that oxygen-plasma treatment alters MIL-125(Ti)-NH_2 band gap and, more significantly, the alignment of highest occupy and lowest unoccupied crystal orbitals. An optimal oxygen plasma treatment to achieve the highest efficiency in water splitting with or without methanol as sacrificial electron donor under UV-Vis or simulated sunlight was determined. The optimized plasma-treated MIL-125(Ti)-NH_2 photocatalyst acts as truly heterogeneous photocatalysts and retains most of its initial photoactivity and crystallinity upon reuse.

Introduction

Metal organic frameworks (MOFs) are being increasingly used as photocatalysts for hydrogen generation and CO2 reduction.[1] Following the lead of TiO_2,[2] Ti-containing MOFs, and particularly MIL-125(Ti) are among the preferred materials, since they combine structural robustness with high photocatalytic activity.[3] Recently, our group has reported the photocatalytic activity of MIL-125(Ti)-NH_2 to promote overall water splitting under both UV-Vis or visible light irradiation.[4] The visible light response of the photocatalyst is introduced to the presence of the amino group on the terephthalate ligand. The highest occupied crystal orbital (HOCO, 2.40 eV) is located at the 2-aminoterephthalate while lowest unoccupied crystal orbital (LUCO, -0.05 eV) at the Ti 3d orbitals.[5] Therefore, MIL-125(Ti)-NH_2 accomplish the thermodynamically requirements for H2O oxidation to O_2 (1.23 eV vs NHE) and H_2O reduction to H_2 (0 eV vs NHE) and allow to perform the overall water splitting under visible light irradiation.[6] Transient absorption spectroscopy and EPR measurements have provided evidence that upon photoexcitation with the appropriate wavelength, electron transfer from the organic ligand to the Ti(IV) metal nodes leading to the formation of a positive hole on the organic linker and a Ti(III) species takes place.[7]

There is a continuous need in increasing the efficiency of the photocatalytic systems to reach the long standing goal of industrial application. In this context, van der Voort and others have shown that defect engineering as a methodology to increase the photocatalytic activity.[8] Plasma treatment is a general technique to modify catalysts, generating defects in their structure.[9] For instance plasma treatment of graphenes increases their catalytic activity.[10] In one precedent of plasma treatment in MOFs, a low-temperature NH_3-plasma treatment was applied to decompose a Ni-based MOF into Ni nanocrystals encapsulated in a thin overlayer of N-doped carbon and further applied for H_2 evolution during water electrolysis in alkaline solution.[11] A milder treatment would be advisable to find the compromise between defect generation while maintaining MOF crystallinity.[1a]

The present study reports the low-power, oxygen plasma treatment of well-known MIL-125(Ti)-NH_2 photocatalyst, showing that just a few minutes treatment increases its photocatalytic efficiency for overall water splitting by a factor of 2. Characterization data indicates that plasma treatment causes terephthalate decarboxylation and these defects shifts to more negative potentials the LUMO energy, resulting in a stable and reusable optimized photocatalyst.

Results and Discussion

3.1. Photocatalyst preparation and characterization

As commented, the aim of this work is to study the influence of the defect-induced oxygen plasma treatment on pristine MIL-125(Ti)-NH_2 on the photocatalytic activity for the water splitting. After several trials, an optimized oxygen plasma treatment at 10 W power was able to generate defects on MIL-125(Ti)-NH_2 in relatively short times (min). Figure 1 shows that the oxygen-plasma treated MIL-125(Ti)-NH_2 solids retains their crystallinity after the plasma treatment at 5, 10 and 15 min.

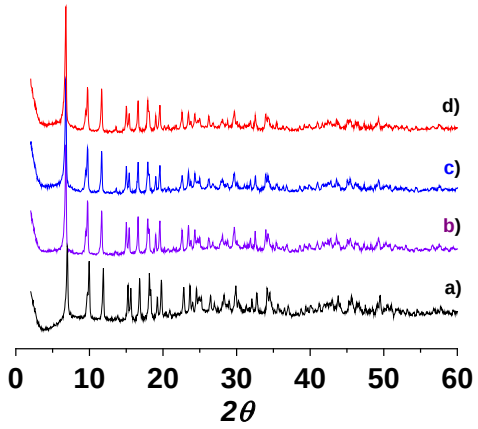

Figure 1. XRD of MIL-125(Ti)-NH_2 (a), MIL-125(Ti)-NH_2-5m (b), MIL-125(Ti)-NH_2-10m (c), MIL-125(Ti)-NH_2-15m (d).

The density of defects induced by the oxygen plasma treatment was conveniently quantified by thermogravimetric analyses (TGA) of the plasma-treated MIL-125(Ti)-NH_2 samples (Figure S1). The MIL-125(Ti)-NH_2 treated for 5 and 10 min with oxygen-plasma exhibits a decrease of the organic content with a concomitant increase of Ti content respect to the pristine MIL-125(Ti)-NH_2 material. In contrast, the MIL-125(Ti)-NH_2 sample treated with oxygen plasma for 15 min shows a Ti content lower than pristine MIL-125(Ti)-NH_2. TGA data was employed to estimate the experimental MIL-125(Ti)-NH_2 formulae (Table 1) of the different samples under study and their deviation respect to the ideal one $(Ti_8O_8)(OH)_4(C_6H_3C_2O_4NH_2)_6$.[12]

Isothermal N_2 adsorption measurements of plasma-treated MIL-125(Ti)-NH_2 solids shows that plasma treatment decreases somehow the BET and pore volume values respect to the pristine MIL-125(Ti)-NH_2 material (Table 1). SEM measurements also show the occurrence of morphological changes, especially the decrease of MIL-125(Ti)-NH_2 average particle size as the plasma treatment time increases (Table 1 and Figures S2-S3).

Table 1. List of MIL-125(Ti)-NH_2 samples studied in this work including their experimental formula, [a] BET and pore volume[b] and average particle size[c].

	Experimental formula	BET / pore volume	MOF average particle size and standard deviation (nm)
MIL-125(Ti)-NH_2	$(Ti_{8.1}O_{8.74})(OH)_{3.83}(C_6H_3C_2O_4NH_2)_{5.40}$	1150 / 0.53	470 ± 219
MIL-125(Ti)-NH_2 5 min	$(Ti_{9.37}O_{5.16})(OH)_{0.831}(C_6H_3C_2O_4NH_2)_4$	956 / 0.43	408 ± 205
MIL-125(Ti)-NH_2 10 min	$(Ti_{11.11}O_{10.2})(OH)_{0,2}(C_6H_3C_2O_4NH_2)_{3.52}$	922 / 0.42	282 ± 86
MIL-125(Ti)-NH_2 15 min	$(Ti_{6.66}O_{6.11})(OH)_{3.19}(C_6H_3C_2O_4NH_2)_{4.86}$	914 / 0.42	242 ± 108

[a] Based on TGA data from Figure S1.

[b] Based on isothermal N_2 adsorption.

[c] Based on SEM measurements from Figure S3.

In order to get some insight on the effect of the oxygen plasma treatment on structure of MIL-125(Ti)-NH_2 solid, XPS and FT-IR analyses of the different samples under study were performed. Figures S4-S7 collect the corresponding XP spectra with the best fitting to each individual component present. The XPS C 1s peak of pristine MIL-125(Ti)-NH_2 shows two bands centred at 284.4 and 289 eV, corresponding to the aromatic carbons and the carboxylate groups of the 2-amino terephthalate organic ligand, respectively. In addition, O 1s XPS shows a broad signal that can be deconvoluted into two individual bands at 534 and 529 eV characteristic of the titanol groups (Ti-OH) present in the metal nodes and the carboxylate oxygen atoms, respectively. N 1s XPS show a main band at 399 eV corresponding to the amino group, accompanied by a smaller signal at 402 eV attributable to the partially protonated amino group. The Ti 2p XPS is constituted by two bands centred at 458 and 465 eV, characteristic of Ti 2p3/2 and Ti 2p1/2 of the Ti^{4+} ions at the metal node of the MOF.

Comparison of the XP spectra of the pristine and oxygen-plasma treated MIL-125(Ti)-NH_2 samples reveal a decrease of the relative intensities of the C 1s band at 289 eV and O 1s band at 539 eV indicating that the oxygen plasma-treatment induces partial decarboxylation (Figure 2). In agreement with these observations, the XPS O 1s peak of the oxygen plasma-treated samples exhibits a relative higher proportion of Ti-OH groups respect to carboxylate O atoms that agrees with the occurrence of decarboxylation.

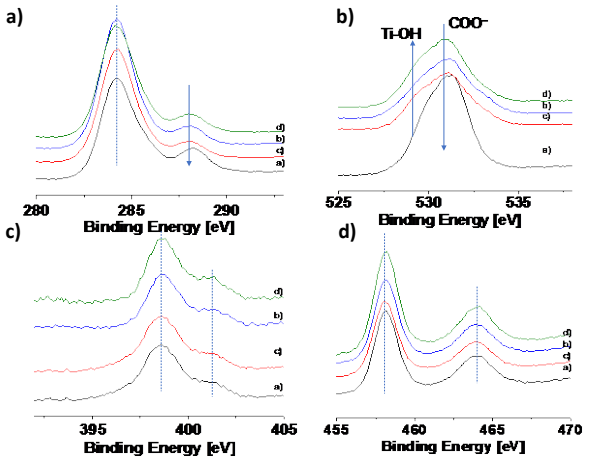

Figure 2. High-resolution XPS peaks of C1s (a), O1s (b), N1s (c) and Ti 2p (d) elements for MIL-125(Ti)-NH_2 (a), MIL-125(Ti)-NH_2-5m (b), MIL-125(Ti)-NH_2-10m (c), MIL-125(Ti)-NH_2-15m (d).

Comparison of FT-IR spectra of the MIL-125(Ti)-NH2 series clearly shows that the oxygen plasma treatment generates an intense band at 3.420 cm^{-1} attributable of the –OH vibration of the titanol groups formed in the decarboxylation process. FT-IR spectroscopy shows that the remaining carboxylate groups do not undergo any shift during the plasma treatment.

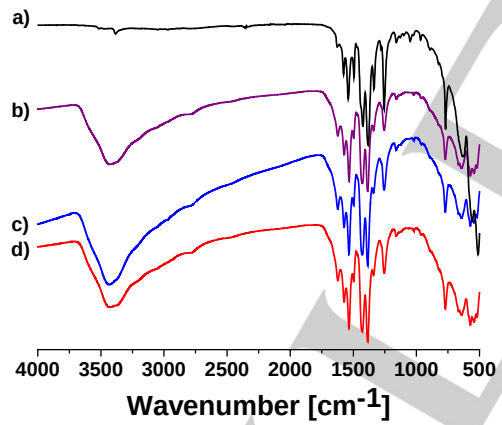

Figure 3. FT-IR of MIL-125(Ti)-NH2 (a), MIL-125(Ti)-NH2-5m (b), MIL-125(Ti)-NH2-10m (c), MIL-125(Ti)-NH2-15m (d).

Overall, the characterization data indicates that the main effect of oxygen plasma treatment of MIL-125(Ti)-NH_2 is the partial decarboxylation of terephthalate ligand, maintaining the crystal structure of the treated solid and with some decrease in the porosity. Figure 4 shows a simplified illustration of the ideal MIL-125(Ti)-NH_2 sample and defective MIL-125(Ti)-NH_2 materials resulting by plasma treatment.

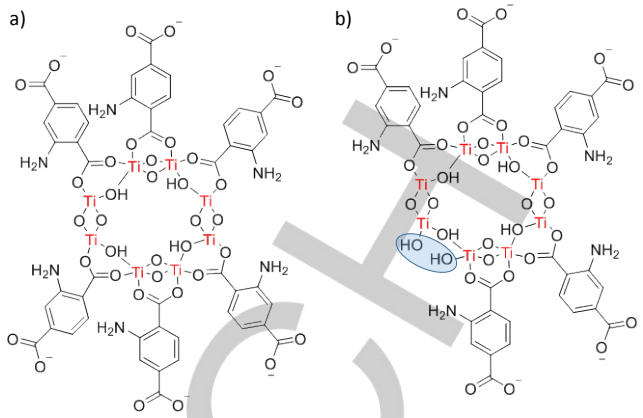

Figure 4. Simplified illustration of ideal (a) and oxygen plasma treated (b) MIL-125(Ti)-NH_2 materials

From the photocatalytic point of view it is relevant to determine if the generation of defects is reflected in variation on the energy levels of the highest occupied and lowest unoccupied crystal orbitals (HOCO and LUCO, respectively). These possible variations were addressed by analysing diffuse reflectance UV-Vis spectra (Figure S8) and valence band energy determined by XPS (Figure S9). In general, diffuse reflectance UV-Vis spectra show one band centred at 280 nm due to the Ti-O ligand-to-metal charge transfer together with a band at 390 nm related to the charge transfer from the 2-aminoterephthalate organic ligand to the oxo-titanium metal node. The Tauc plot was used to calculate the band gap for the series of solids, observing small differences in all samples, oxygen plasma treatment slight increasing its value. XPS was employed to estimate the valence band edge of the different materials.[13] Table 2 collects the band gap, HOCO and LUCO energy values estimated for the different MIL-125(Ti)-NH2 solids under study. Regardless the similar band gap values of the different samples, significant differences between HOCO and LUCO energies were determined. As it will be commented later the energy band alignment strongly influences the resulting photocatalytic activity for the water splitting.

Table 2. Influence of the oxygen plasma treatment on the electronic alignment of the MIL-125(Ti)-NH_2 solids.

Sample	Estimated band gap (eV)	HOCO (eV)	LUCO (eV)
MIL-125(Ti)-NH_2	2.64	2.34	-0.30
MIL-125(Ti)-NH_2 5 min	2.81	2.18	-0.62
MIL-125(Ti)-NH_2 10 min	2.71	2.40	-0.31
MIL-125(Ti)-NH_2 15 min	2.76	1.85	-0.91

3.2. Photocatalytic activity

3.2.1. Photocatalytic overall water splitting

Since it has been proposed that structural defects can influence positively the photocatalytic activity,[8] and considering the relevance of robust MIL-125(Ti)-NH_2 as visible light photocatalyst, [4, 5b, 12, 14] it was of interest to experimentally address the possible influence of plasma treatment on the photocatalytic activity for overall water splitting. Aimed at this purpose, a systematic study of the photocatalytic activity of the series of MIL-125(Ti)-NH_2 samples in overall water splitting under the same conditions was undertaken. Figure 5a shows that the oxygen plasma treatment gradually increases the efficiency of the overall water splitting for MIL-125(Ti)-NH_2 under UV-Vis irradiation with an optimum for 10 min of treatment. Attempts to prolong the oxygen plasma treatment beyond 15 min on MIL-125(Ti)-NH_2 resulted in a decrease of photoactivity. It is remarkable that the optimized MIL-125(Ti)-NH_2-10m sample exhibits double photocatalytic activity than pristine MIL-125(Ti)-NH_2. It should be noted that the photoactivity of MIL-125(Ti)-NH_2-10m is even higher than an analogous MIL-125(Ti)-NH_2 sample incorporating RuOx nanoparticles as co-catalyst (69 mmol g^{-1} in 22 h) under analogous reaction conditions.[4] Worth noting is that the present results reconfirm the ability of MIL-125(Ti)-NH_2 to promote O_2 generation from H_2O. This point was further proved in an experiment using labelled $H_2{}^{18}O$, whereby the formation of $^{18}O_2$ (m/z 36 mau) was monitored by mass spectrometry as the only O2 species (Figure S12).

The same trend of photocatalytic activity was observed under visible light irradiation (λ >450 nm) (Figure 5b) for the overall water splitting with the sample MIL-125(Ti)-NH_2-10m being the most active. These experiments under visible light irradiation indicate that a large percentage of the observed photoactivity derives from the visible zone of the radiation spectrum. Importantly, the most active oxygen plasma treated MIL-125(Ti)-NH_2 sample exhibits good photocatalytic activity (Figure 5c) and reusability (Figure 5d) under simulated sunlight irradiation, maintaining its crystallinity as revealed by XRD (Figure S10). The heterogeneity of the reaction was confirmed that observing that once H_2 and O_2 gases are evolving from water, if the solid is removed by filtration and the system allowed react further under the same photocatalytic reaction conditions, no additional gas evolution occurs (Figure S11).

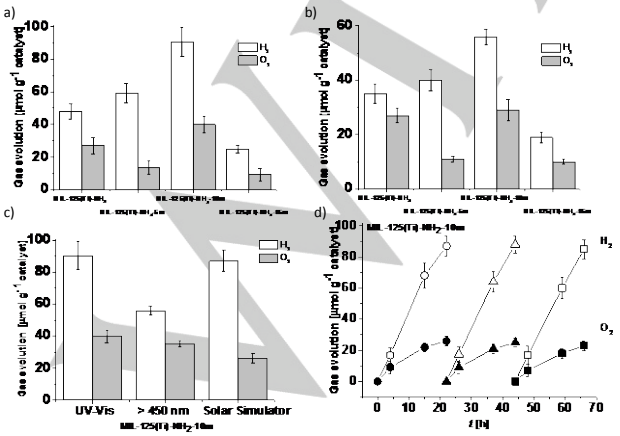

Figure 5. Overall water splitting using MIL-125(Ti)-NH_2 materials as photocatalysts under UV-Vis (a), visible (I> 450) and simulated sunlight irradiation for three consecutive cycles (c, d). General reaction conditions: photocatalyst (20 mg), H_2O (20 mL), 35 ºC, irradiation source (Xe lamp 150 W equipped or not with 450 nm filter or solar simulator of 1 sun) reaction time 22 h.

The increase of photoactivity upon oxygen plasma treatment of MIL-125(Ti)-NH_2-5m and MIL-125(Ti)-NH_2-10m can be explained considering that the samples with slightly higher band gap values exhibit a more positive HOCO and negative LUCO values respect to the pristine MIL-125(Ti)-NH_2 solid (Table 2 and Figure 6). Furthermore, the smaller average particle size of the MIL-125(Ti)-NH_2 samples treated at 5 and 10 min should also be beneficial for light harvesting respect to the bigger crystals of pristine MIL-125(Ti)-NH_2. In contrast, the MIL-125(Ti)-NH_2-15m sample with the longer treatment affecting more pronouncedly the structure shows the lowest photocatalytic activity of all the samples in the series. This observation can be explained considering that MIL-125(Ti)-NH_2-15m sample exhibits the less oxidizing HOCO and, thus, the thermodynamically and kinetically most difficult half-reaction H_2O oxidation to O_2 is less favoured.

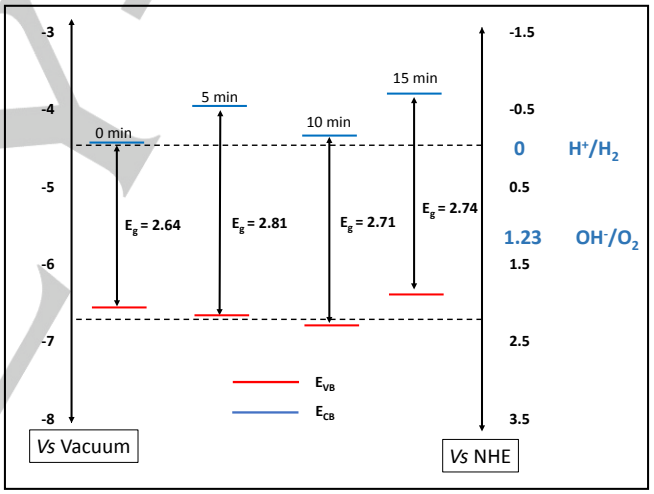

Figure 6. Energy levels of the MIL-125(Ti)-NH_2 samples without (0 min) or with oxygen plasma treatment (5 min, 10 min and 15 min) under vacuum of NHE as reference

3.2.2. Photocatalytic water splitting in the presence of methanol.

A series of experiments of photocatalytic hydrogen generation in the presence of methanol as electron donor was also carried out comparing the efficiency of pristine and oxygen plasma-treated MIL-125(Ti)-NH_2 samples. In this case, all the oxygen-plasma treated samples exhibited higher H_2 production than the pristine MIL-125(Ti)-NH_2 sample under UV-Vis irradiation (Figure 7a). This observation can be understood according to Figure 6 considering that all the oxygen plasma treated MIL-125(Ti)-NH_2 samples exhibit lower LUCO values than pristine MIL-125(Ti)-NH_2. The highest H_2 generation activity for MIL-125(Ti)-NH_2-10m with less negative LUMO and higher particle size respect to MIL-125(Ti)-NH_2-15m can be explained considering the higher ability

of MIL-125(Ti)-NH_2-10m to promote methanol oxidation than MIL-125(Ti)-NH_2-15m and, thus, higher H_2 evolution.

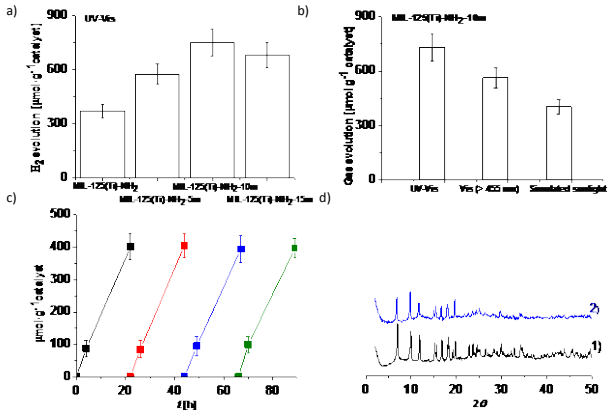

Figure 7. Photocatalytic hydrogen generation in the presence of methanol using several MIL-125(Ti)-NH_2 materials under UV-Vis irradiation (a), Visible light (l>450 nm) (b) and simulated sunlight irradiation (c) for several reuses (c). Panel d) shows the XRD of the fresh (1) and three times used (2) MIL-125(Ti)-NH_2-10m photocatalyst. General reaction conditions: photocatalyst (20 mg), H_2O (20 mL), irradiation source (Xe lamp 150 W equipped or not with 450 nm filter), 35 ºC, reaction time 22 h

Importantly, the higher photocatalytic activity of the optimized oxygen-plasma treated MIL-125(Ti)-NH_2-10m for H_2 generation in the presence of methanol also occurs under visible (λ >455 nm) and simulated sunlight irradiation (Figure 7b). Furthermore, the MIL-125(Ti)-NH_2-10m maintains its photoactivity under simulated sunlight irradiation after several reuses (Figure 7c) and retains its crystallinity as revealed by XRD (Figure 7d).

To further support the higher activity of oxygen-plasma treated MIL-125(Ti)-NH_2 samples to promote reduction reactions respect to pristine MIL-125(Ti)-NH_2, methyl viologen (MV^{2+}, E0 = -0.44 V, pH independent) was used as probe molecule. MV^{2+} is commonly used in photochemistry as electron acceptor rendering a visually observable blue coloured radical cation stable under inert atmosphere.[15]

In the present case, it was observed that all the MIL-125(Ti)-NH_2 samples tested in this work promote MV^{2+} reduction to the coloured $MV^{+\cdot}$ radical cation. Figure 8a illustrates the one electron reduction of MV^{2+} to $MV^{+\cdot}$ using MIL-125(Ti)-NH_2-10m. Interestingly, the photocatalytic activity of oxygen-plasma treated MIL-125(Ti)-NH_2 samples follows for the photocatalytic MV^{2+} reduction the same trend respect to pristine MIL-125(Ti)-NH_2 than that previously observed in the photocatalytic water splitting or hydrogen generation (Figure 8b). Thus, it seems that the more negative LUCO reduction potential values of plasma-treated MIL-125(Ti)-NH_2 samples increases their ability to promote reduction reactions respect to pristine MIL-125(Ti)-NH_2.

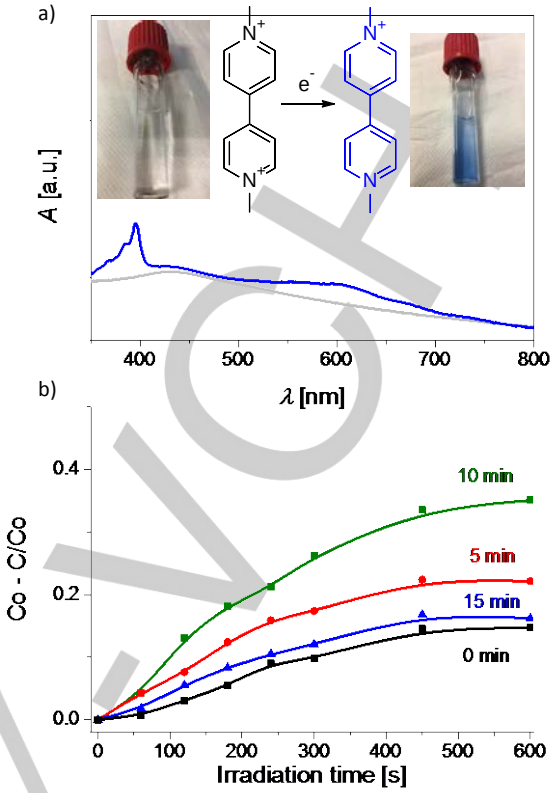

Figure 8. a) UV-vis spectra and photographs of Ar-purged acetonitrile suspension of MIL-125(Ti)-NH_2-10m containing MV^{2+} in ethanol before (grey line) and after (blue line) irradiation with a Xe lamp. The blue colour indicates to the presence of $MV^{+\cdot}$ formed by one electron reduction of MV^{2+}. b) Temporal evolution of the concentration of $MV^{+\cdot}$ upon irradiation.

3.2.2. Reaction mechanism / Photoelectrochemical measurements

The previous results indicates the higher photocatalytic activity of MIL-125(Ti)-NH_2-10m for the overall water splitting, H2 evolution and MV2+ reduction. These results fit with the calculated changes in the HOCO and LUCO band energy alignment caused by plasma treatment. In addition, the MIL-125(Ti)-NH_2-10m sample has smaller average particle size than the pristine MIL-125(Ti)-NH_2 solid, favouring diffusion and light harvesting.

In order to further insights on the optimal photocatalytic activity of oxygen-plasma treated MIL-125(Ti)-NH_2-10m sample respect to the pristine MIL-125(Ti)-NH_2 solid, the photocurrent response of MIL-125(Ti)-NH_2-10m on FTO electrodes was measured. [16] Figure 9 shows that the photocurrent intensity increases as the polarization voltage increases. Interestingly, the onset potential for MIL-125(Ti)-NH_2-10m is somewhat smaller by 0.1 V respect to pristine MIL-125(Ti)-NH_2 material (see insets of Figure 9). This observation agrees with the shift in the HOCO-LUCO band energy values measured by XPS and absorption spectroscopy upon plasma treatment. Furthermore, a higher photocurrent increase was observed upon addition of methanol when using MIL-125(Ti)-NH_2-10m respect to pristine MIL-125(Ti)-NH_2. This observation agrees with the higher photocatalytic H2 production

measured for MIL-125(Ti)-NH_2-10m respect to MIL-125(Ti)-NH_2 in the presence of methanol as sacrificial electron donor.

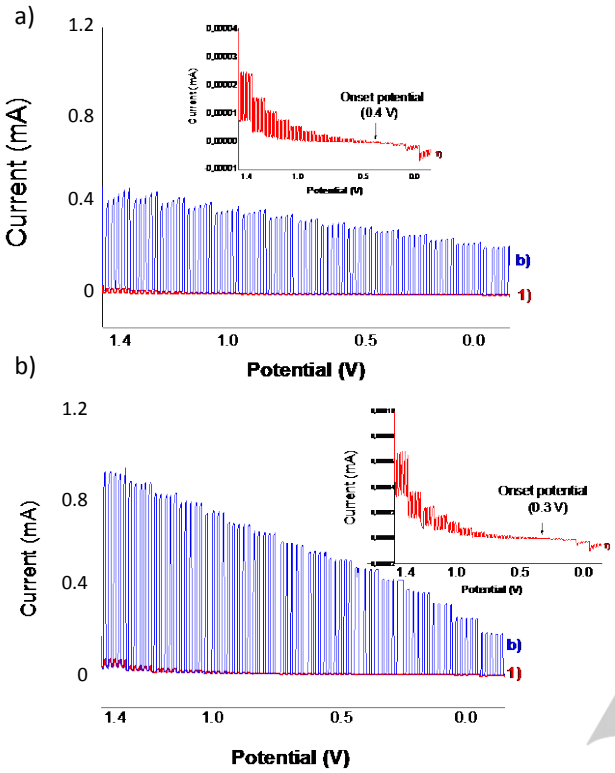

Figure 9. Photocurrent intensity versus polarization potential measured for the pristine MIL-125(Ti)-NH_2/FTO (a) or MIL-125(Ti)-10m/FTO (b) electrode in a deoxygenated $TBAPF_6$ (0.1 M) acetonitrile solution in the absence (1, red line) or in the presence (b, blue line) of methanol upon 300 W Xe lamp illumination. The insets show a magnification of the photoresponse in the absence of methanol, with indication of the onset potential.

Conclusion

The present study shows that oxygen plasma treatment on the benchmark MIL-125(Ti)-NH_2 material generates structural defects that induces electronic changes resulting in the formation of an optimized solid with enhanced photocatalytic activity. Characterization data by PXRD and isothermal N_2 adsorption reveal that plasma treated MIL-125(Ti)-NH_2 solids retain crystallinity in a large extent, diminishing somewhat BET and pore volume. XPS, FT-IR and thermogravimetric analyses have shown that plasma treatment on MIL-125(Ti)-NH_2 induces partial decarboxylation and concomitant Ti-OH formation. Diffuse reflectance UV-Vis spectroscopy and valence band determination shows the alteration of the band energy values. Importantly, optimized MIL-125(Ti)-NH_2-10m solid exhibits superior photocatalytic activity for overall water splitting and hydrogen evolution in the presence of methanol as sacrificial agent respect to the pristine MIL-125(Ti)-NH_2. In summary, this work provides evidence of the influence of structural defects on the photocatalytic activity proposed in theoretical studies and shows a strategy to further increase the photocatalytic activity of MOFs through defect engineering by plasma treatment.

Experimental Section

2.1. Materials

All the chemicals and reagents used in this work were of analytical or HPLC grade and supplied by Merck.

2.2. Synthesis of MIL-125(Ti)-NH_2

MIL-125(Ti)-NH_2 was prepared by a solvothermal method as previously reported.[16] Briefly, 2-aminoterephthalic acid (1.43 g, 7.9 mmol) was dissolved in anhydrous N,N-dimethylformamide (DMF, 20 mL) and, then, anhydrous methanol (5 mL) was added to the flask. The system was sonicated for 20 min and, then, transferred to a Teflon-lined autoclave (50 mL). Subsequently, titanium isopropoxide (1.36 g, 4.8 mmol) was added and the autoclave was sealed and heated up to 110 °C for 72 h. The system was cooled down to room temperature and the resulting precipitate was recovered by filtration, washed with DMF at room temperature for 12 h under stirring and, then, washed with DMF at 120 °C for 12 h. The same washing procedure was repeated using methanol as solvent. Finally, the solid was recovered by filtration and dried in an oven at 100 °C.

2.3. Oxygen plasma treatment

Oxygen plasma treatment of MIL-125(Ti)-NH_2 was carried out using a commercially available, low-pressure plasma FEMTO (Diener) instrument. Briefly, a certain amount of sample (100 mg) weighed on a crucible was introduced in the plasma chamber. The chamber was firstly degassed under vacuum for 30 min and, then, an O_2 flow was introduced achieving after 5 min a stable and constant pressure of 4 mbar. An optimized potential of 10 W was found to be appropriate to generate structural defects on the MIL-125(Ti)-NH_2 material in relatively short times (5, 10 and 15 min). Finally, the plasma chamber was submitted to vacuum for 5 min and then, refilled with Ar until atmospheric pressure was reached.

2.4. Catalyst characterization

Powder X-ray diffractograms (PXRD) of plasma-treated MIL-125(Ti)-NH_2 samples were recorded in a Philips XPert diffractometer (40 kV and 45 mA) using Ni filtered Cu Kα radiation. Diffuse reflectance UV-visible spectra of the solids were recorded in a Cary 5000 Varian spectrophotometer with an integrating sphere where the sample as compressed powder was placed in a sample holder. X-ray photoelectron spectra (XPS) were recorded using a SPECS spectrometer equipped with a MCD-9 detector using a monochromatic Al (Kα= 1486.6 eV) X-ray source. Spectra deconvolution was performed after Shirley subtraction of background with the CASA software using the C 1s peak at 284.4 eV as binding energy reference. Fourier-transform infrared (FTIR) spectra were recorded on compressed powders using a Bruker spectrophotometer in an attenuated total reflectance (ATR) cell. The morphology of the MOF samples was characterized using a scanning electron microscope (SEM, Zeiss instrument, AURIGA Compact). MOF particle size distribution was estimated for each sample by measuring more than 300 particles. Isothermal N_2 adsorption measurements of the MIL-125(Ti) solids were carried out using an ASAP 2010 Micromeritics station.

2.6. Photocatalytic water splitting experiments

All the experiments were carried out at least in triplicate. The presented data points corresponds to the average of the independent measurements and the error bar corresponds to the standard deviation. The photocatalytic water splitting experiments were carried out in the absence or in the presence of methanol as sacrificial electron donor. Briefly, 20 mg of catalyst was dispersed in 20 mL of distilled H_2O or a mixture of H_2O (18 mL) and methanol (2 mL) using a quart reactor (51 mL) and the system sonicated for 20 min to obtain a good solid

dispersion. Then, the system was purged with Ar for 1 h. The suspension under stirring was irradiated with a Xe lamp (150 W). In some cases a cut-off filter (λ >450 nm) was employed to ensure visible light irradiation. In other experiments irradiations were carried out under simulated sunlight irradiation (OrielTM, 1 sun power).

The evolved gases from the different experiments were analysed by withdrawing from the head space several aliquots at different reaction times. Then, the reaction aliquots were injected into an Agilent 490 Micro GC system (Molsieve 5 Å column using Ar as carrier gas). The temperature of the reactor was monitored and the pressure was analysed by means of a manometer.

2.7. Methyl viologen (MV^{2+}) experiments

Photoinduced electron transfer measurements were carried out using MOF dispersions (0.2 mg/mL) in water/methanol mixtures (9:1 vol:vol) containing acetonitrile solution of MV^{2+} (0.15 mM). The MOF dispersions containing MV^{2+} were sonicated, placed in quartz cuvette capped with septa and bubbling Ar for 5 min prior irradiation. The cuvettes containing the MOF dispersions under Ar atmosphere were irradiated with a Hg-Xe lamp (150 W) for different times and measuring the UV-Vis absorbance with a Cary 50 Conc UV-Vis spectrophotometer. The photoinduced electron transfer measurements were followed by the increase of the absorption band centered near 400 nm and corresponding to the $MV^{\cdot+}$ radical cation.

2.8. Photocurrent measurements

Photocurrent measurements were carried out in a standard three-electrode electrochemical cell using a transparent fluoride-doped tin oxide (FTO)-coated glass substrate coated with a thin layer of the corresponding MIL-125(Ti)-NH_2 sample (FTO-MIL-125(Ti)-NH_2). The FTO-MIL-125(Ti)-NH_2 films were employed as working electrode, a platinum wire as the counter electrode and a standard calomel electrode (SCE) as the reference electrode. Prior to the measurement, the oxygen present in the cell was removed by bubbling an Ar stream through the electrolyte. The photocurrent was measured under dark and under illumination upon polarizing the working electrode at potentials from 1.4 to -0.2 V. Irradiation was performed using an optical fibber connected to a 300 W Xe lamp.

Acknowledgements

S.N. thanks financial support by the Fundación Ramón Areces (XVIII Concurso Nacional para la Adjudicación de Ayudas a la Investigación en Ciencias de la Vida y de la Materia, 2016), Ministerio de Ciencia, Innovación y Universidades RTI 2018-099482-A-I00 project and Generalitat Valenciana grupos de investigación consolidables 2019 (ref: AICO/2019/214) project. Financial support by the Spanish Ministry of Science, Innovation and Universities (Severo Ochoa and RTI2018-098237-B-C21) and Generalitat Valenciana (Prometeo 2017-083) is also gratefully acknowledged.

Keywords: metal-organic frameworks; visible-light photocatalysis; defect engineering; overall water splitting; hydrogen generation.

[1] a) A. Dhakshinamoorthy, A. M. Asiri, H. García, *Angew. Chem. Int. Ed.* **2016**, *55*, 5414-5445; b) A. Dhakshinamoorthy, Z. Li, H. Garcia, *Chem. Soc. Rev.* **2018**, *47*, 8134-8172; c) T. Zhang, W. Lin, *Chem. Soc. Rev.* **2014**, *43*, 5982-5993; d) W. Wang, X. Xu, W. Zhou, Z. Shao, *Adv. Sci.* **2017**, *4*, 160037; e) J.-L. Wang, C. Wang, W. Lin, *ACS Catal.* **2012**, *2*, 2630-2640; f) M. Wen, K. Mori, Y. Kuwahara, T. An, H. Yamashita, *Chem. Asian J.* **2018**, *13*, 1767-1779; g) M. Ding, R. W. Flaig, H.-L. Jiang, O. M. Yaghi, *Chem. Soc. Rev.* **2019**, *48*, 2783-2828; h) D. Li, M. Kassymova, X. Cai, S.-Q. Zang, H.-L. Jiang, *Coord. Chem. Rev.* **2020**, *412*, 213262; i) T. Zhang, Y. Jin, Y. Shi, M. Li, J. Li, C. Duan, *Coord. Chem. Rev.* **2019**, *380*, 201-229; j) H. Luo, Z. Zeng, G. Zeng, C. Zhang, R. Xiao, D. Huang, C. Lai, M. Cheng, W. Wang, W. Xiong, Y. Yang, L. Qin, C. Zhou, H. Wang, Y. Zhou, C. Tian, **2020**, *383*, 123196.

[2] a) J. Schneider, M. Matsuoka, M. Takeuchi, J. Zhang, Y. Horiuchi, M. Anpo, D. W. Bahnemann, *Chem. Rev.* **2014**, *114*, 9919-9986; b) A. Fujishima, T. N. Rao, D. A. Tryk, *J. Photochem. Photobiol. C: Photochem. Rev.* **2000**, *1*, 1-21; cA. Fujishima, X. Zhang, D. A. Tryk, *Surf. Sci. Rep.* **2008**, *63*, 515-582.

[3] a) J. Zhu, P.-Z. Li, W. Guo, Y. Zhao, R. Zou, *Coord. Chem. Rev.* **2018**, *359*, 80-101; b) X. Chen, X. Peng, L. Jiang, X. Yuan, H. Yu, H. Wang, J. Zhang, Q. Qi Xia, *Chem. Eng. J.* **2020**, *395*, 125080; c) Q. Wang, Q. Gao, A. M. M. Al-Enizi, A. Nafadyc, S. Ma, *Inorg. Chem. Front.* **2020**, *7*, 300-339.

[4] S. Remiro-Buenamañana, M. Cabrero-Antonino, M. Martínez-Guanter, M. Álvaro, S. Navalón, H. García, *Appl. Catal. B. Environ.* **2019**, 677-684.

[5] a) Y. An, B. Xu, Y. Liu, Z. Wang, P. Wang, Y. Dai, X. Qin, X. Zhang, B. Huang, *ChemistryOpen* **2017**, *6*, 701 – 705; b) C. H. Hendon, Tiana, D., Fontecave, M., Sanchez, C., D'arras, L., Sassoye, C., Rozes, L., Mellot-Draznieks, C. and Walsh, A., *J. Am. Chem. Soc.* **2013**, *135*, 10942-10945.

[6] T. Hisatomi, K. Domen, *Nat. Catal.* **2019**, *2*, 387–399.

[7] M. A. Nasalevich, C. H. Hendon, J. G. Santaclara, K. Svane, B. van der Linden, S. L. Veber, M. Fedin, A. J. Houtepen, M. A. van der Veen, F. Kapteijn, A. Walsh, J. Gascon, *Sci. Rep.* **2016**, *6*, 23676.

[8] a) X. Ma, L. Wang, Q. Zhang, H.-L. Jiang, *Angew. Chem. Int. Ed.* **2019**, *58*, 12175 –12179; b) A. De Vos, Hendrickx, K., Van Der Voort, P., Van Speybroeck, V. and Lejaeghere, K., *Chem. Mater.* **2017**, *29*, 3006-3019; c) M. Taddei, Schukraft, G. M., Warwick, M. E. A., Tiana, D., McPherson, M.J., Jones, D.J and Petit, C., *J. Mater. Chem. A.* **2019**, *7*, 23781-23786; d) K. L. Svane, J. K. Bristow, J. D. Gale, A. Walsh, *J. Mater. Chem.* **2018**, *6*, 8507-8513; eK. Hendrickx, D. E. P. Vanpoucke, K. Leus, K. Lejaeghere, A. V. Van Yperen-De Deyne, V. Van Speybroeck, P. Van Der Voort, K. Hemelsoet, *Inorg. Chem.* **2015**, *54*, 10701-10710.

[9] Z. Wang, Y. Zhang, E. C. Neyts, X. Cao, X. Zhang, B. W.-L. Jang, C.-j. Liu, *ACS Catal.* **2018**, *8*, 2093–2110.

[10] A. Primo, A. Franconetti, M. Magureanu, N. B. Mandache, C. Bucur, C. Rizescu, B. Cojocaru, V. I. Parvulescu, H. Garcia, *Green Chem.* **2018**, *20*, 2611-2623.

[11] Y. Guo, X. Gao, C. Zhang, Y. Wu, X. Chang, T.,, T. Wang, X. Zheng, A. Du, B. Wang, J. Zheng, K. K. Ostrikovc, X. Li, *J. Mater. Chem. A* **2019**, *7*, 8129-8135.

[12] M. Dan-Hardi, C. Serre, T. Frot, L. Rozes, G. Maurin, C. Sanchez, G. Ferey, *J. Am. Chem. Soc.* **2009**, *131*, 10857-10859.

[13] Y. Peng, A. Rendón-Patiño, A. Franconetti, J. Albero, A. Primo, H. García, *ACS Appl. Energy Mater.* **2020**, *3*, 6623-6632.

[14] A. Melillo;, M. Cabrero-Antonino;, S. Navalón;, M. Álvaro;, B. Ferrer;, H. García, *Applied Catalysis B: Environmental* **2020**, *278*.

[15] a) T. W. Ebbesen, G. Ferraudi, *J. Phys. Chem.* **1983**, 3717–3721; b) H. Garcia, S. Navalon, *Metal-Organic Frameworks: Applications in Separations and Catalysis, Wiley, ISBN: 978-3-527-80910-3* **2018**.

[16] A. A. Babaryk, O. R. C. Almengor, M. Cabrero-Antonino, S. Navalón, H. García, P. Horcajada, *Inorg. Chem.* **2020**, *59*, 3406–3416.

Entry for the Table of Contents

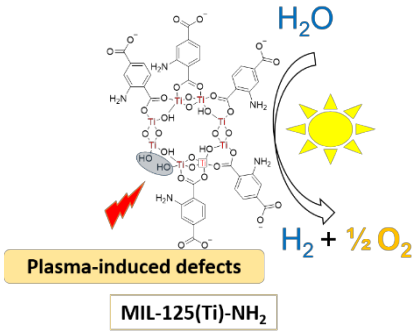

WILEY-VCH